

Conjoint Effect of Boron Nitride and Surface-Enhanced Flake Graphite in Thermal Conductivity of Thermally Conductive Grease

Xiaojun Xiong¹ and Yifan Li^{1,2,*}

¹School of Energy and Materials, Shanghai Polytechnic University, Shanghai, 201209, China

²Shanghai Engineering Research Center of Advanced Thermal Functional Materials, Shanghai Polytechnic University, Shanghai, 201209, China

Abstract: The next generation of high-power electronic devices is expected to exhibit improved heat dissipation capabilities despite their smaller size. Current studies have investigated the utilization of hybrid fillers, our study introduces a novel approach by combining boron nitride (BN) and surface-enhanced flake graphite (G), both of which possess a platelet-like structure, to develop a thermally conductive grease. The grease shows an exceptionally high thermal conductivity of 2.21 W/mK and an extremely low electrical conductivity of 7.3×10^{-6} S/m. The viscosity of the grease is measured at 149 Pa·s. By incorporating hybrid fillers with a significantly high aspect ratio into EPON 828, a notable reduction of interfacial thermal resistance is observed, which is attributed to the formation of an effective pathway for phonon transfer facilitated by the unique characteristics of the hybrid fillers. Various theoretical models are employed to corroborate the experimental data, which facilitates substantiating the fundamental principles underlying the enhanced thermal conductivity of the prepared thermal grease.

Keywords: Boron Nitride, Graphite, Thermally Conductive Grease, Electric Conductivity, Viscosity.

1. INTRODUCTION

The trend of rapidly miniaturizing electronic devices while enhancing their power capabilities has gained significant momentum. A notable example is the reduction in size from a 25.4 mm square die for the Pentium 2 processor to a mere 12.5 mm square die for the Pentium 4. This size reduction occurred even though the Pentium 4 dissipates up to 80 W of power, whereas the Pentium 2 only dissipates 33 W [1]. The denser packaging of active components or microelectronics within electronic devices is a crucial factor in miniaturizing the devices and advancing the development of high-performance systems [2]. Denser packaging of components is only feasible when there is the efficient and rapid removal of unwanted heat from the heat source to the heat sink. This heat transfer occurs through the process of thermal conduction between the heat source and the heat sink [3]. Even a slight increase in the operating temperature, typically on the order of 10-15 °C, at the junction of electronic devices can lead to a significant reduction in their lifespan. Such a temperature increment can result in a two-fold decrease in the expected lifespan of the devices [4]. Indeed, it can be stated that the reliability of electronic devices is exponentially influenced by the operating temperature of the junction. The higher the operating temperature, the greater the impact on

device reliability and lifespan [5]. Therefore, it is critical to efficiently and promptly remove unwanted heat from the heat source of electronic devices. This ensures that the devices can operate smoothly at the desired temperature [6].

The most commonly employed method to dissipate unwanted heat from electronic devices is by attaching a heat sink to the devices [3, 6, 7]. The effectiveness of thermal conduction is influenced by the quality of thermal contact between the heat source (electronic devices) and the heat sink [8]. However, the performance of the heat sink in scattering the unwanted heat is often constrained by interfacial resistance caused by non-surface flatness and surface irregularities on both the heat source and the heat sink [9]. Surface irregularities on the heat source and heat sink can result in the entrapment of air within the gap between them. This trapped air acts as a barrier to efficient thermal conduction due to its low thermal conductivity, typically around 0.026 W/m.K [10]. The common method to reduce interfacial resistance between the contact points is to introduce an additional layer of material as shown in Figure 1. The additional material is thermal interface material (TIM), which provides an effective pathway for thermal conduction [6, 11]. TIMs can take various forms, including thermal fluids, solders, phase change materials, and thermal grease (paste). Among these options, thermal grease based on polymers such as silicone and epoxy is the most commonly used thermal interface material [12, 13].

*Address correspondence to this author at the Shanghai Engineering Research Center of Advanced Thermal Functional Materials, Shanghai Polytechnic University, Shanghai, 201209, China; E-mail: liyf@sspu.edu.cn

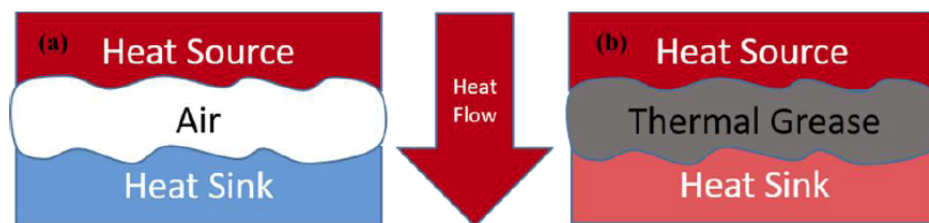


Figure 1: (a) Surface roughness filled with air, (b) Surface roughness filled with TIM (thermal grease).

Various types of TIMs have been developed by reinforcing polymer matrix or silicone with highly thermally conductive and electrically insulating fillers, including materials such as boron nitride, aluminum nitride, alumina, or silica [14, 15]. Higher thermal conductivity in TIMs leads to improved thermal conduction between the heat source and the heat sink. In addition to high thermal conductivity, TIMs should possess a low coefficient of thermal expansion (CTE) and be easily deformable under small contact pressure. These properties enable the TIMs to effectively conform to and make contact with all the irregular areas of the mating surfaces [16].

Thermal grease offers favorable heat transfer performance even under minimal contact pressure, which can be applied in a thin layer at the junction [17]. It typically consists of two main components: a polymer base and a thermally conductive filler. The kinematic viscosity of the polymer base ranges from 112 to 770 mm²/s at 40 °C. Epoxies have gained significant popularity as a matrix material for coatings, adhesives, and composites [18]. They are high-performance thermosetting resins known for their exceptional mechanical and adhesion properties, thermal stability, high electrical insulation capabilities, affordability, and ease of processing [19, 20]. Epoxy resins have a very low thermal conductivity of around 0.2 W/mK that can be further enhanced by adding high thermally conductive fillers [21]. The preferred volume percentage of filler in a thermal grease is about 55 to 78%. Ceramic fillers with high thermal conductivity and nearly electrically insulative like boron nitride, aluminum nitride, alumina, and silicon carbide are widely used [22, 23]. While metallic fillers can significantly increase the thermal conductivity of thermal grease, the manufacturing cost associated with producing metallic filler-based greases is usually high. Additionally, such greases do not provide electrical insulation, which could lead to electric shocks if used in electronic devices.

In this study, thermal greases were formulated by combining epoxy (EPON 828) with different loadings of

boron nitride (BN) as a filler. The loadings of BN ranged up to 60 wt%, and a further increase in the amount of BN will lead to the final failure to obtain a uniform composite resin. Additionally, thermal greases were also prepared by incorporating both BN and surface-enhanced flake graphite (G) as fillers into the EPON 828 resin, with loadings of BN and G up to 38 wt%. The study aimed to explore the synergistic effect of BN and G on the thermal conductivity of the developed thermal greases. To assess the packing density of the fillers used, a two-dimensional (2D) bin packing technique was employed. The 2D packing problem aims to identify the conditions that result in the objective function achieving the optimal value within a discrete and finite mathematical structure [24]. The filler loading in the thermal greases was carefully controlled to ensure that the fluidity of the paste was not compromised [25]. This means that the amount of fillers added was limited to maintain the desired consistency and flow characteristics of the thermal greases. Different theoretical models were studied to validate the experimental data. Maxwell model and Hamilton and Crosser Semi- Theoretical (H&C) model were used to confirm the data for a single filler. Lewis and Nelsen Semi- Theoretical Model (L&M) and (H&C) models were used to authenticate the data for hybrid fillers [26, 27].

2. EXPERIMENTAL

2.1. Materials

Undiluted clear di-functional bisphenol A/epichlorohydrin derived liquid epoxy resin (EPON 828), provided by Hexion Chemicals, was utilized as the matrix material in this project in its as-received form. EPON 828 is renowned for its exceptional mechanical, adhesive, dielectric, and chemical properties, making it a suitable choice for the study. The selection of fillers is crucial in enhancing the thermal conductivity of thermally conductive grease, considering their shape and size. In this project, two different fillers with a similar platelet-like structure but different sizes were employed to improve the thermal

conductivity of EPON 828 and ensure adequate adhesion. PCTP30 BN, provided by Carbo Therm, was selected as one of the fillers, with an average particle size of 30 microns. Additionally, 3775 graphite, provided by Asbury Carbon, was chosen as the other filler, with an average particle size of 44 microns.

2.2. Fillers Properties

BN from CarboTherm is a platelet powder with a structure that is well-suited for thermoplastic polymers. It shares a platy, lamellar structure similar to graphite, which allows it to align with the flow direction during polymer processing [28]. This characteristic makes BN an excellent choice for heat-spreading applications, where efficient heat transfer is desired. Graphite used in the study is natural-based graphite that has undergone exfoliation, calendaring, and sizing processes specifically for thermal management applications [29, 30]. This surface-enhanced flake graphite has a wide range of uses, including conductive seals, mechanical seals, high-purity metal cover carbon, nano-platelet systems, friction systems, coatings, greases, and lubricant additives. Its versatile properties make it suitable for various applications that require enhanced conductivity and lubrication [31]. The properties of the materials including thermal

conductivity (λ), average particle diameter (PD), specific surface area (SSA), and density mentioned above are shown in Table 1.

2.3. Preparation of Thermal Paste

To prepare the thermal grease with a single filler, the process involved several steps. First, the desired weight of the filler was measured using a precise weighing scale and placed in a 30 mL beaker. Then, EPON 828 resin was added in the appropriate quantity to achieve the specific weight ratio specified for the formulation. After adding the resin, the mixture was left at room temperature for 5 hours. This step allowed the filler to become moistened, preventing it from blowing off during the subsequent mixing process using a mechanical stirrer. Once the filler and resin were sufficiently moistened, the sample was mixed using a mechanical mixer (RZR 2021). The mixing process was carried out at a rotation speed of 1800 rpm for 4 hours. The thermal grease with hybrid fillers was prepared using the same procedure as above in which a larger particle (G) was mixed first. The smaller particle (BN) was added to the mixture after four hours. The sample was then mixed for two more hours to obtain the hybrid thermal grease. Thermally conductive grease with hybrid fillers is listed in Table 2 and they are named as

Table 1: Properties of the Epoxy and Thermal Fillers

Materials	Density (g/cm ³)	λ (W/m.K.)	PD (μ m)	SSA (m ² /g)
EPON 828	1.16	0.202	N/A	N/A
G	2.26	230	44.00	17.20
BN	2.10	130	30.00	1.00

Table 2: List of Thermally Conductive Grease with Hybrid Fillers

Sample	BN		Graphite		Total vol% of fillers
	wt%	vol%	wt%	vol%	
B5G33	5.0	2.3	33.0	14.1	16.4
B10G28	10.0	4.6	28.0	11.9	16.5
B15G23	15.0	6.8	23.0	9.8	16.6
B20G18	20.0	9.1	18.0	7.6	16.7
B25G13	25.0	11.4	13.0	5.5	16.9
B15G10	15.0	7.3	10.0	4.5	11.8
B15G15	15.0	7.1	15.0	6.6	13.7
B15G20	15.0	6.9	20.0	8.6	15.5
B15G25	15.0	6.8	25.0	10.5	17.3
B15G30	15.0	6.6	30.0	12.4	19

BxGy, where x and y represent the weight percentage of BN and graphite, respectively.

2.4. Characterization

The morphology of BN and graphite fillers was examined using scanning electron microscopy (SEM) with a JEOL-7401 instrument. This technique allowed for the visualization and analysis of the surface structure and particle size of the fillers. The thermal conductivity of the samples was measured using a thermal conductivity analyzer called C-Therm TCi, which is based on a modified transient plane source method. This method is suitable for measuring the thermal conductivity of solids, liquids, and powders. The analyzer incorporates a curling-type heating source located at the sensor's hub. Heat is generated at the hub and then transferred to the material through the sensor. The voltage decrease at the heating source is rapidly recorded, and the thermal conductivity is calculated based on the decrease in voltage data. The testing range of the instrument is 0-100 W/mK, and it can measure thermal conductivity across a wide temperature range (-50 to 200 °C) with an accuracy better than 5%. The electrical insulation properties of the thermal greases were characterized using a Keithley 2750 instrument and a 2-wire resistivity technique. The electric resistivity was measured by manipulating two probes, with each probe serving as both a current and voltage probe [32]. The viscosity of the thermal greases was determined using a Bohlin Gemini Rheometer equipped with a cone and plate setup. A cone with a 4-degree angle and a 40 mm diameter plate was used for viscosity measurements. The gap distance between the cone and plate was set at 150 µm. To assess heat transfer, a 3-megapixel infrared thermal imaging camera (FLIR E40: 19,200 pixels, Instrumary, USA) was employed. Thermal

images were captured during the heating process, allowing for the visualization and analysis of heat distribution within the thermal paste. The thermal grease and epoxy were applied at the center of an aluminum plate using a 0.8" inner diameter and 1.0" outer diameter O-ring. A DC power supply (PWS2721, Tektronix) was used to heat the aluminum plate, with a constant voltage mode set at 12 V and a current set at 0.32 A.

3. RESULTS AND DISCUSSION

The size and shape of fillers were observed to influence the thermal conductivity of the grease [33]. The morphology of both BN and graphite fillers was examined using a scanning electron microscope (SEM), as shown in Figure 2. It was observed that both BN and graphite exhibited a platelet-like structure, which can contribute to improved thermal conductivity in the grease [34]. The average particle size of BN and graphite was measured from SEM images using Image J software. The average particle size of BN was derived to be 31.2 µm, and the average thickness was 2.01 µm. The average particle size of graphite was 44.9 µm, and the average thickness was 1.9 µm. The aspect ratio (A) was calculated using Equation (1) [35]. The average aspect ratio of BN and G was calculated to be 15.52 and 23.63, respectively from 25 different readings.

$$\text{Aspect Ratio (A)} = \frac{\text{Average Diameter (D)}}{\text{Average Thickness (T)}} \quad (1)$$

The effects of BN and G content on the thermal conductivity of EPON 828-based thermal grease are depicted in Figure 3. It was observed that the thermal conductivity of the thermal grease exhibited a direct correlation with the filler content. Specifically, the thermal conductivity of the thermal grease containing

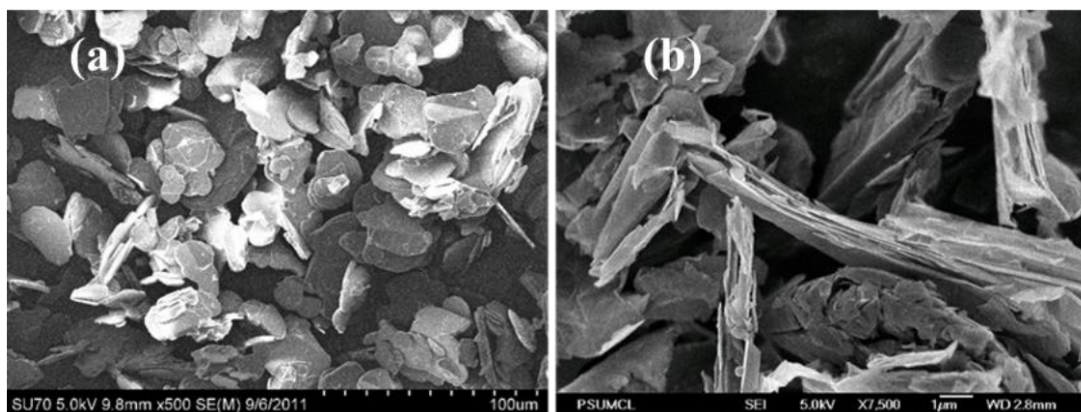


Figure 2: SEM image of (a) BN and (b) graphite.

60 wt% BN in EPON 828 was measured to be 1.01 W/mK, which was five times higher than that of the native EPON 828 (0.202 W/m·K). Similarly, the thermal conductivity of the thermal grease containing 30 wt% graphite in EPON 828 was found to be 1.21 W/mK, six times higher than that of the native EPON 828. However, it should be noted that as the filler content exceeded 60 wt% for BN and 30 wt% for graphite, the mobility of the thermal grease decreased significantly. This decrease in mobility can hinder the dispersion of the filler in EPON 828, thus limiting the formation of an efficient thermal conductivity path. Therefore, it was observed that the thermal conductivity of the thermal grease increased significantly up to 45 wt% of BN and 25 wt% of G. Furthermore, the viscosity of the thermal grease was found to increase with the increased filler content. This higher viscosity can pose challenges in achieving better dispersion of the filler in EPON 828, further affecting the thermal conductivity performance of the grease [36, 37].

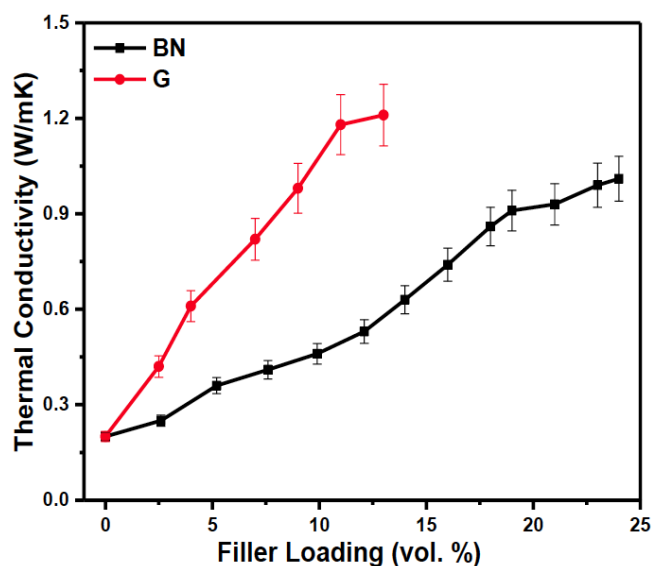


Figure 3: Effects of BN and G content on the thermal conductivity of thermally conductive grease.

Different thermal greases with hybrid fillers were prepared by varying the weight percentage of BN and graphite to determine the optimal ratio between the two fillers. The total weight percentage of fillers was maintained at 38 wt% to ensure the desired mobility of the thermal grease. Figure 4 illustrates the thermal conductivity of the thermal grease as a function of the weight fraction of the small particle (BN) while keeping the total weight fraction of hybrid fillers (BN&graphite) constant at 38 wt%.

It was observed that beyond 38 wt% of hybrid fillers, the mobility of the thermal grease decreased during the

mixing process, leading to limited dispersion of fillers in EPON 828. Within the studied weight fractions, the thermal conductivity of the thermal grease filled with hybrid fillers increased as the weight fraction of the small particle (BN) increased, reaching a maximum of 15 wt%. The maximum thermal conductivity achieved was 2.21 W/mK when the total fillers comprised 38 wt%, with 15 wt% being BN and 23 wt% being graphite. This value was nearly ten times higher than that of native EPON 828. Notably, the thermal conductivity of neat EPON 828 increased by 994%. These results indicate that the optimal weight ratio between the large and small particles improves the packing volume and enhances the thermal conductivity of the thermal grease.

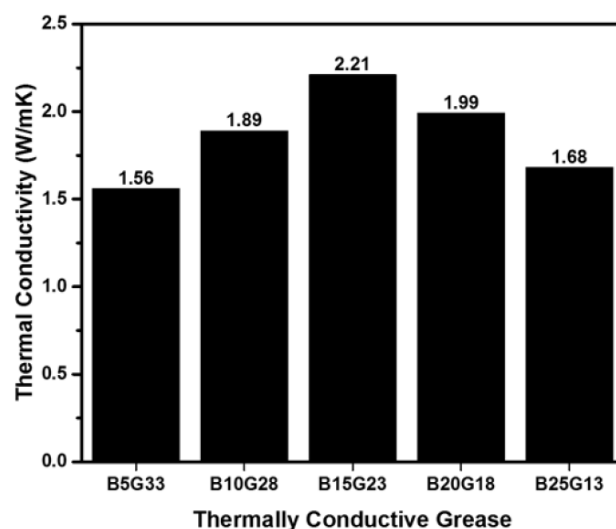


Figure 4: Effect of hybrid fillers on thermal conductivity of thermally conductive grease.

The optimal ratio of BN and graphite, which directly corresponds to the packing density, was verified using the 2D bin packing technique. The coordinates of BN and graphite were generated using AutoCAD, taking into account the average particle diameter of BN and graphite, as shown in Figure 5. A regular hexagon was drawn inside a circle with a specific diameter. The circle was divided into six equal parts using the "divide" command, and lines were drawn to form a hexagon. The ratio of BN to graphite was set such that BN was fixed at 15 while graphite ranged from 5 to 30, referring to Figure 4.

The bin size was selected to accommodate the combination of BN and graphite with minimal wastage. The waste area of the bin was calculated as shown in Table 3, reflecting the packing density of the combination, as they are directly proportional to each other. The area of graphite was calculated as 1257.5

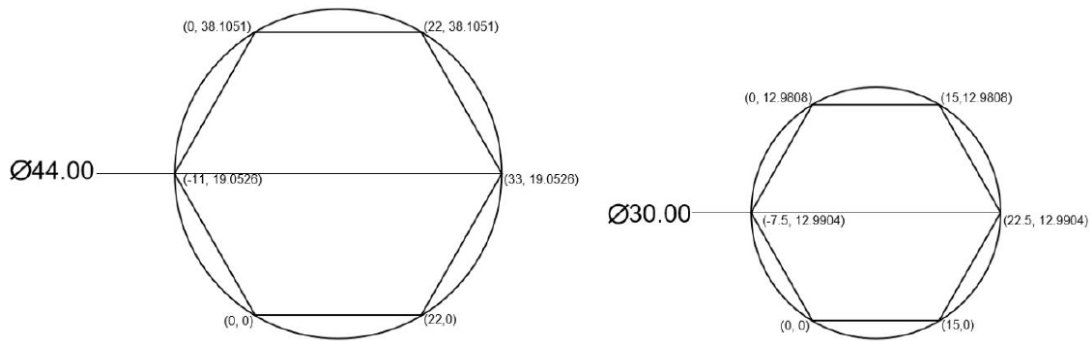


Figure 5: Illustration of the coordinates of graphite and BN.

Table 3: Results from 2D Bin Packing

Sample	Area of Bin	Area of BN & graphite	Waste area	Ratio
B15G5	23,870	15,055.9	8,814.4	0.36
B15G10	31,329	21,343.2	9,985.8	0.31
B15G15	40,401	27,630.5	12,770	0.31
B15G20	48,029	33,917.3	14,111.7	0.29
B15G25	58,081	40,205.2	17,875.8	0.30
B15G30	69,696	46,492.6	23,203.4	0.33

unit square, and the area of BN was calculated as 584.6 unit square. The minimal waste area is achieved when the number of graphite fillers falls between 20 and 25, with BN fixed at 15. A minimal waste area ratio indicates a dense packing of fillers, indicating a higher packing density [38]. Figure 6 presents a graphical image obtained from the 2D bin packing of 30 graphite and 15 BN, illustrating the arrangement of the fillers within the bin.

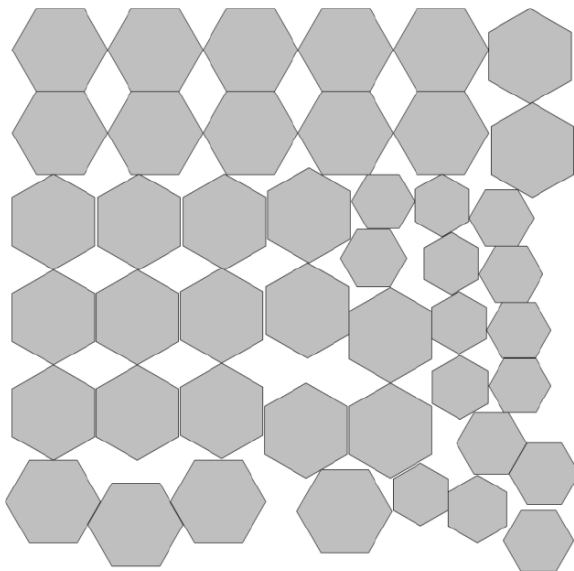


Figure 6: Image from 2D bin packing of 30 graphite and 15 BN.

Thermal conductivity models can be used to predict the thermal conductivity of greases containing thermally conductive fillers. Hamilton and Crosser Semi-Theoretical Model (H&C) was used to predict the thermal conductivity of thermally conductive grease with a single filler, which considers the integral thermal conductivities, the concentration of each integral, the aspect ratio, orientation, and packing of the filler, shown as Equation (2) [39, 40]:

$$K = K_c * \frac{K_d + (n-1) * K_c - (n-1) * \phi * (K_c - K_d)}{K_d + (n-1) * K_c + \phi * (K_c - K_d)} \quad (2)$$

n is an empirical constant, calculated by Equation (3):

$$n = \frac{3}{\phi} \quad (3)$$

ϕ is the sphericity. The sphericity is defined as the surface area of a sphere, with a volume equal to that of the particle, to the surface area of the particles. The parameter n for BN and G was calculated from Equation (2). Different thermally conductive greases were prepared with single filler at very low loading (1 to 15 wt%) and thermal conductivity was measured in the lab. The measured thermal conductivity was used to back calculate n for each grease and average n was calculated. Calculated n was used to predict the thermal conductivity of thermally conductive grease.

Figure 7 shows the comparison between theoretical model and experimental value.

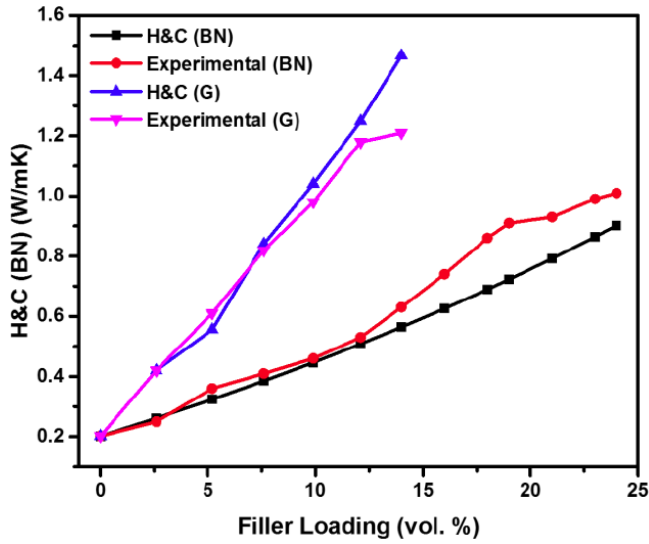


Figure 7: Comparison between the theoretical model and experimental value.

Lewis and Nielsen Semi-Theoretical Model (L&N) was used to predict the thermal conductivity of thermally conductive grease with hybrid filler. This model accounts for integral thermal conductivities, the concentration of each integral, the aspect ratio, orientation, and packing of the filler. Equation (4) was used to predict the thermal conductivity of grease with hybrid filler:

$$K = k_1 * \frac{(1 + (A * B * \phi)i)}{(1 - (B * \varphi * \phi)i)} \tag{4}$$

B is calculated by Equation (5)

$$B = \frac{(k_2 - 1)}{k_1} / \left(\frac{k_2}{k_1} + A \right) \tag{5}$$

k_1 is the thermal conductivity of the matrix, k_2 is the thermal conductivity of the filler, φ is the filler volume fraction. A is the shape and orientation factor, and B is a factor that takes into account the relative thermal conductivity of the two components. φ is given by Equation (6):

$$\varphi = 1 + \frac{1 - \phi_m}{\phi_m^2} * \phi \tag{6}$$

ϕ_m is the maximum packaging fraction of the filler. φ relates to the maximum packing fraction and the filler volume fraction. A and ϕ_m were taken from the tables

listed elsewhere [41]. A was taken as 1.5 for BN considering it as a sphere and A for G was supposed to be 15. The maximum packaging fraction of BN was taken to be 74% considering it as a sphere and packing close to hexagonal packing. Equation (7) below is used to compare theoretical and experimental values.

$$\varepsilon = \frac{\sum_{i=1}^n (x_i - y_i)^2}{\sum_{i=1}^n x_i^2} \tag{7}$$

ε is defined as a standardized lack of fit term and quantifies how the theoretical model compares to the experimental data. x_i is the experimental thermal conductivity and y_i is the calculated thermal conductivity.

After predicting the theoretical thermal conductivity (k_{th}) from Nielsen’s model, a correction factor of $-1.79 + 1.91 * k_{th}$ was applied to correct the gap during extrapolation from the theoretical to the experimental model. The correction factor was obtained from linear regression [42]. Figure 8 shows the comparison of thermal conductivity between the theoretical model and the experimental. The standardized lack of a fit term for thermal grease with hybrid filler was calculated to be 0.11 using the experimental model. A value of $\varepsilon = 0$ indicates a perfect fit of the experimental data with the model.

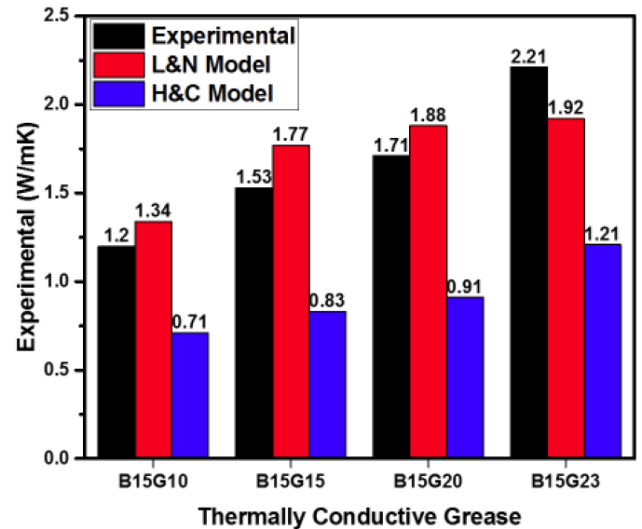


Figure 8: Comparison of thermal conductivity between the theoretical and experimental values.

The thermal grease used in electronic devices needs to maintain electrical insulation properties to prevent electric shocks [43]. This is achieved by incorporating electrically insulating fillers (such as BN) and a polymer matrix (EPON 828) in the thermal

grease formulation. The electric conductivity of a sample containing 25 wt% of graphite (G) and 15 wt% of BN was measured to be 7.3×10^{-6} S/m. As shown in Figure 9, the electric conductivity of the thermally conductive grease increases in direct proportion to the loading of electrically conductive fillers (in this case, graphite filler, 3775 G).

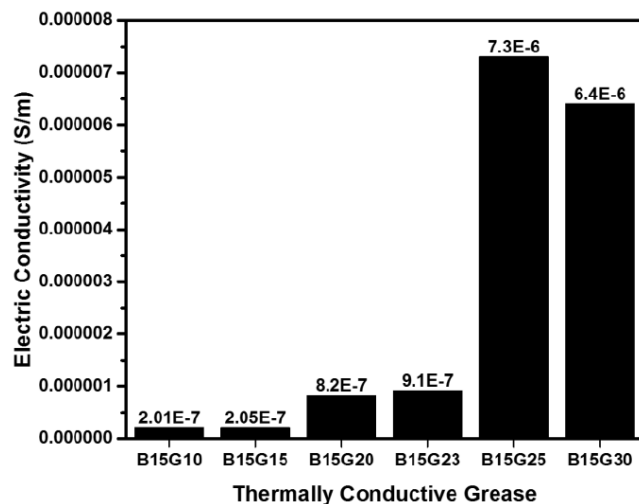


Figure 9: Effect of G on the electrical conductivity of the thermally conductive grease.

Thermal grease is required to exhibit high thermal performance even under small contact pressure, allowing for minimal thickness application at the junction. It should maintain its mobility to effectively fill all the air gaps between the heat source and heat sink, creating a continuous pathway for thermal conduction [44, 45]. Additionally, thermally conductive grease should not separate, run, migrate, or bleed from the contact points. The viscosity of commonly used thermally conductive grease, such as Arctic Silver 5, was measured to serve as a reference for characterizing the viscosity of our own thermally conductive greases. The viscosity of Arctic Silver 5 was found to be 145 Pa·s. As shown in Figure 10, the viscosity of thermally conductive grease is directly proportional to the filler loading.

Thermal imaging using a three-megapixel infrared camera was employed to capture thermal images of the samples during the heating process. Thermal images of pure epoxy and the thermal grease (B15G23) were taken at 30-second intervals for 5 minutes. The results indicated that the thermal grease exhibited faster heating compared to the pure epoxy, as depicted in Figure 11. This observation demonstrates that the thermally conductive grease facilitates the rapid dissipation of heat from the heat

source to the heat sink. After 5 minutes of heating, the maximum temperature reached by EPON 828 was 66.3 °C, while the thermal grease reached a maximum temperature of 72.4 °C. It was observed that EPON 828 started to leak out from the O-ring once the temperature reached 51.5 °C, whereas the thermally conductive grease remained intact. This observation highlights the superior thermal stability of the thermally conductive grease compared to pure EPON 828.

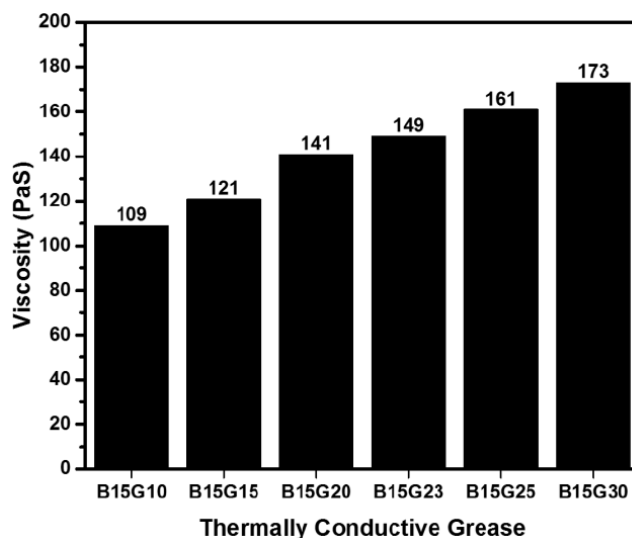


Figure 10: Effect of filler on the viscosity of the thermally conductive grease.

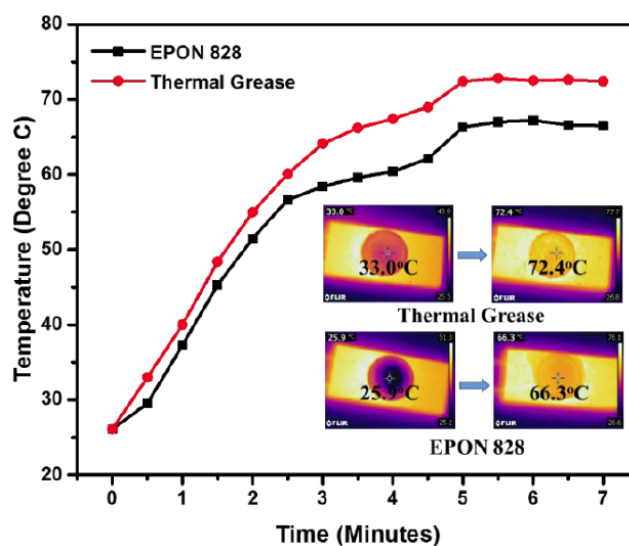


Figure 11: Temperature rampage of EPON 828 and thermally conductive grease.

4. CONCLUSIONS

In summary, our study stands out due to the utilization of a unique combination of BN and G, both possessing a platelet-like structure, in the development

of thermally conductive grease. The results indicate that at low filler content, BN particles disperse randomly with weak interactions among each other. However, as the filler content increases, the probability of forming a thermal conductivity path increases, resulting in higher thermal conductivity of the thermally conductive grease. The introduction of hybrid fillers BN and G significantly enhances the thermal conductivity of the grease. This can be attributed to the smaller BN particles filling the gaps left by the larger graphite particles. Consequently, interfacial phonon scattering and thermal resistance are effectively reduced, leading to an increase in thermal conductivity. The electric conductivity of the thermally conductive grease is directly proportional to the loading of the electrically conductive filler. Preserving the mobility of the thermal grease is crucial to ensure it can effectively fill the air gaps between the heat source and the heat sink, thereby providing a pathway for efficient thermal conduction. The thermally conductive grease developed in this study fulfills these criteria. Consequently, there is a need for further research on a larger scale to address heating issues in electronic devices.

ACKNOWLEDGEMENT

The authors acknowledge funding from the Shanghai Dawn Plan (22CGA78) and Shanghai Sailing Program (21YF1414200), the Discipline of Shanghai-Materials Science and Engineering, and the Shanghai Engineering Research Center of Advanced Thermal Functional Materials.

REFERENCES

- [1] Gwinn JP, Webb RL. Performance and testing of thermal interface materials. *Microelectronics J* 2003; 34: 215-222. [https://doi.org/10.1016/S0026-2692\(02\)00191-X](https://doi.org/10.1016/S0026-2692(02)00191-X)
- [2] Charles Jr HK. Miniaturized electronics. *Johns Hopkins APL Tech Dig* 2005; 26: 402-413.
- [3] Leong C-K, Chung D. Carbon black dispersions as thermal pastes that surpass solder in providing high thermal contact conductance. *Carbon* 2003; 41: 2459-2469. [https://doi.org/10.1016/S0008-6223\(03\)00247-1](https://doi.org/10.1016/S0008-6223(03)00247-1)
- [4] Viswanath R, Wakharkar V, Watwe A, Lebonheur V. Thermal performance challenges from silicon to systems. *Intel Technology Journal* 2000; 4: 1-16.
- [5] Li Y, Xu H, Zhang Y, *et al.* Paving 3D interconnected $C_{ring}-C_3N_4@rGO$ skeleton for polymer composites with efficient thermal management performance yet high electrical insulation. *Int Commun Heat Mass Transf* 2022; 135: 106147. <https://doi.org/10.1016/j.icheatmasstransfer.2022.106147>
- [6] Sim LC, Ramanan S, Ismail H, Seetharamu K, Goh T. Thermal characterization of Al_2O_3 and ZnO reinforced silicone rubber as thermal pads for heat dissipation purposes. *Thermochim Acta* 2005; 430: 155-165. <https://doi.org/10.1016/j.tca.2004.12.024>
- [7] Xu Y, Luo X, Chung D. Sodium silicate based thermal interface material for high thermal contact conductance. *J Electron Packag* 2000; 122: 128-131. <https://doi.org/10.1115/1.483144>
- [8] Luo X, Xu A, Yunsheng, Chung D. Thermal stability of thermal interface pastes, evaluated by thermal contact conductance measurement. *J Electron Packag* 2001; 123: 309-311. <https://doi.org/10.1115/1.1371925>
- [9] Lee S. How to Select a Heat Sink. *Advanced Thermal Engineering*, Aavid Thermal Technologies. Inc., Laconia 1996.
- [10] Yu W, Xie H, Yin L, Zhao J, Xia L, Chen L. Exceptionally high thermal conductivity of thermal grease: Synergistic effects of graphene and alumina. *Int J Therm Sci* 2015; 91: 76-82. <https://doi.org/10.1016/j.ijthermalsci.2015.01.006>
- [11] Chiu CP, Solbrekken GL, Chung YD. Thermal modeling of grease-type interface material in PPGA application[C]// Thirteenth Annual IEEE. Semiconductor Thermal Measurement and Management Symposium. IEEE, 1997: 57-63. <https://doi.org/10.1109/STHERM.1997.566783>
- [12] Chung D. Thermal interface materials. *J Mater Eng Perform* 2001; 10: 56-59. <https://doi.org/10.1361/105994901770345358>
- [13] Li Y, Zhang T, Zhang Y, Zhao C, Zheng N, Yu W. A comprehensive experimental study regarding size dependence on thermal conductivity of graphene oxide nanosheet. *Int Commun Heat Mass* 2022; 130: 105764. <https://doi.org/10.1016/j.icheatmasstransfer.2021.105764>
- [14] Rimdusit S, Ishida H. Development of new class of electronic packaging materials based on ternary systems of benzoxazine, epoxy, and phenolic resins. *Polymer* 2000; 41: 7941-7949. [https://doi.org/10.1016/S0032-3861\(00\)00164-6](https://doi.org/10.1016/S0032-3861(00)00164-6)
- [15] Yu S, Hing P, Hu X. Thermal conductivity of polystyrene-aluminum nitride composite. *Compos Part A Appl Sci Manuf* 2002; 33: 289-292. [https://doi.org/10.1016/S1359-835X\(01\)00107-5](https://doi.org/10.1016/S1359-835X(01)00107-5)
- [16] Xu Y, Chung D, Mroz C. Thermally conducting aluminum nitride polymer-matrix composites. *Compos Part A Appl Sci Manuf* 2001; 32: 1749-1757. [https://doi.org/10.1016/S1359-835X\(01\)00023-9](https://doi.org/10.1016/S1359-835X(01)00023-9)
- [17] Zhang Y, Li Y, Dong L, *et al.* Robust Smart Fabrics Composed of MgO Nanostructures Encapsulated in Hollow Polystyrene Fibers for Efficient Thermoregulation. *ACS Appl Nano Mater* 2022; 5: 16831-16841. <https://doi.org/10.1021/acsnanm.2c03787>
- [18] Kong J, Tang Y, Zhang X, Gu J. Synergic effect of acrylate liquid rubber and bisphenol A on toughness of epoxy resins. *Polym Bull* 2008; 60: 229-236. <https://doi.org/10.1007/s00289-007-0862-x>
- [19] Gu J, Zhang Q, Dang J, Zhang J, Chen S. Preparation and mechanical properties researches of silane coupling reagent modified β -silicon carbide filled epoxy composites. *Polym Bull* 2009; 62: 689-697. <https://doi.org/10.1007/s00289-009-0045-z>
- [20] Gu J, Zhang Q, Dang J, Xie C. Thermal conductivity epoxy resin composites filled with boron nitride. *Polym Adv Technol* 2012; 23: 1025-1028. <https://doi.org/10.1002/pat.2063>
- [21] Yung KC, Liem H. Enhanced thermal conductivity of boron nitride epoxy-matrix composite through multi-modal particle size mixing. *J Appl Polym Sci* 2007; 106: 3587-3591. <https://doi.org/10.1002/app.27027>
- [22] Zhou W, Qi S, Tu C, Zhao H, Wang C, Kou J. Effect of the particle size of Al_2O_3 on the properties of filled heat-conductive silicone rubber. *J Appl Polym Sci* 2007; 104: 1312-1318. <https://doi.org/10.1002/app.25789>

- [23] Sarvar F, Whalley DC, Conway PP. Thermal interface materials-A review of the state of the art[C]//2006 1st electronic system integration technology conference. IEEE, 2006, 2: 1292-1302.
<https://doi.org/10.1109/ESTC.2006.280178>
- [24] Martello S, Vigo D. Exact solution of the two-dimensional finite bin packing problem. *Manage Sci* 1998; 44: 388-399.
<https://doi.org/10.1287/mnsc.44.3.388>
- [25] Li Y, Mehra N, Ji T, *et al.* The stiffness-thermal conduction relationship at the composite interface: The effect of particle alignment on the long-range confinement of polymer chains monitored by scanning thermal microscopy. *Nanoscale* 2018; 10: 1695-1703.
<https://doi.org/10.1039/C7NR06780A>
- [26] Mu L, He J, Li Y, *et al.* Molecular origin of efficient phonon transfer in modulated polymer blends: Effect of hydrogen bonding on polymer coil size and assembled microstructure. *J Phys Chem C* 2017; 121: 14204-14212.
<https://doi.org/10.1021/acs.jpcc.7b03726>
- [27] Mu L, Li Y, Mehra N, Ji T, Zhu J. Expedited phonon transfer in interfacially constrained polymer chain along self-organized amino acid crystals. *ACS Appl Mater Interfaces* 2017; 9: 12138-12145.
<https://doi.org/10.1021/acsami.7b02257>
- [28] Zhao C, Li Y, Liu Y, Xie H, Yu W. A critical review of the preparation strategies of thermally conductive and electrically insulating polymeric materials and their applications in heat dissipation of electronic devices. *Advanced Composites and Hybrid Materials* 2023; 6: 1-26.
<https://doi.org/10.1007/s42114-022-00584-2>
- [29] Mehra N, Mu L, Ji T, Li Y, Zhu J. Moisture driven thermal conduction in polymer and polymer blends. *Compos Sci Technol* 2017; 151: 115-123.
<https://doi.org/10.1016/j.compscitech.2017.08.010>
- [30] Mehra N, Li Y, Yang X, *et al.* Engineering molecular interaction in polymeric hybrids: Effect of thermal linker and polymer chain structure on thermal conduction. *Compos B Eng* 2019; 166: 509-515.
<https://doi.org/10.1016/j.compositesb.2019.02.029>
- [31] Mehra N, Jeske M, Yang X, *et al.* Hydrogen-bond driven self-assembly of two-dimensional supramolecular melamine-cyanuric acid crystals and its self-alignment in polymer composites for enhanced thermal conduction. *ACS Appl Polym Mater* 2019; 1: 1291-1300.
<https://doi.org/10.1021/acsapm.9b00111>
- [32] Schroder DK. *Semiconductor material and device characterization*. John Wiley & Sons 2015.
- [33] Liu Y, Zhang Y, Li Y, Zhang T, Xie H, Yu W. Flexible cellulose composite film incorporated by carbon nitride@ graphene oxide prepared by a "compressed-aerogel" approach for efficient thermal management. *Ceram Int* 2023.
<https://doi.org/10.1016/j.ceramint.2023.01.131>
- [34] Dong L, Li Y. Experimental identification of topography-based artifact phenomenon for micro-/nanoscale thermal characterization of polymeric materials in scanning thermal microscopy. *AIP Adv* 2022; 12: 045311.
<https://doi.org/10.1063/5.0088360>
- [35] Ng HY, Lu X, Lau SK. Thermal conductivity of boron nitride-filled thermoplastics: effect of filler characteristics and composite processing conditions. *Polym Compos* 2005; 26: 778-790.
<https://doi.org/10.1002/pc.20151>
- [36] Zhang L, Pan J, Cabrera ED, *et al.* Highly oriented graphitic networks grown by chemical vapor deposition as thermal interface materials. *Ind Eng Chem Res* 2020; 59: 22501-22508.
<https://doi.org/10.1021/acs.iecr.0c04519>
- [37] Li Y, Zhang Y, Liu Y, Xie H, Yu W. A comprehensive review for micro/nanoscale thermal mapping technology based on scanning thermal microscopy. *J Therm Sci* 2022; 31: 976-1007.
<https://doi.org/10.1007/s11630-022-1654-1>
- [38] Mehra N, Li Y, Zhu J. Small organic linkers with hybrid terminal groups drive efficient phonon transport in polymers. *J Phys Chem C* 2018; 122: 10327-10333.
<https://doi.org/10.1021/acs.jpcc.8b01991>
- [39] Nielsen LE. The thermal and electrical conductivity of two-phase systems. *Ind Eng Chem Fundam* 1974; 13: 17-20.
<https://doi.org/10.1021/i160049a004>
- [40] Hauser RA, Keith JM, King JA, Holdren JL. Thermal conductivity models for single and multiple filler carbon/liquid crystal polymer composites. *J Appl Polym Sci* 2008; 110: 2914-2923.
<https://doi.org/10.1002/app.28869>
- [41] Weber EH, Clingerman ML, King JA. Thermally conductive nylon 6, 6 and polycarbonate based resins. II. Modeling *J Appl Polym Sci* 2003; 88: 123-130.
<https://doi.org/10.1002/app.11572>
- [42] Guo M, Kashfipour MA, Li Y, Dent RS, Zhu J, Maia JM. Structure-Rheology-Property relationships in double-percolated Polypropylene/Poly (methyl methacrylate)/Boron nitride polymer composites. *Compos Sci Technol* 2020; 198: 108306.
<https://doi.org/10.1016/j.compscitech.2020.108306>
- [43] Li Y, Mehra N, Ji T, Zhu J. Realizing the nanoscale quantitative thermal mapping of scanning thermal microscopy by resilient tip-surface contact resistance models. *Nanoscale Horiz* 2018; 3: 505-516.
<https://doi.org/10.1039/C8NH00043C>
- [44] Li Y, Lin H, Mehra N. Identification of thermal barrier areas in graphene oxide/boron nitride membranes by scanning thermal microscopy: thermal conductivity improvement through membrane assembling. *ACS Appl Nano Mater* 2021; 4: 4189-4198.
<https://doi.org/10.1021/acsanm.1c00528>
- [45] Zhang Y, Li Y, Lei Q, Fang X, Xie H, Yu W. Tightly-packed fluorinated graphene aerogel/polydimethylsiloxane composite with excellent thermal management properties. *Compos Sci Technol* 2022; 220: 109302.
<https://doi.org/10.1016/j.compscitech.2022.109302>

Received on 26-04-2023

Accepted on 05-05-2023

Published on 08-06-2023

<https://doi.org/10.6000/1929-5995.2023.12.04>

© 2023 Xiong and Li; Licensee Lifescience Global.

This is an open access article licensed under the terms of the Creative Commons Attribution License (<http://creativecommons.org/licenses/by/4.0/>) which permits unrestricted use, distribution and reproduction in any medium, provided the work is properly cited.